# Instabilities of rotating inclined buoyancy layers

Y. Xiao,[1,2] J. J. Tao,[1,*] and F. H. Busse[3]

[1]*Department of Mechanics and Engineering Science, College of Engineering, Peking University, Beijing 100871, People's Republic of China*

[2]*School of Civil Engineering, Shandong University, Jinan 250061, People's Republic of China*

[3]*Institute of Physics, University of Bayreuth, Bayreuth 95440, Germany*

(Received 7 March 2023; accepted 20 July 2023; published 15 August 2023)

The boundary layer near a cooled inclined plate, which is immersed in a stably stratified fluid rotating about an axis parallel to the direction of gravity, is a model for katabatic flows at high latitudes. In this paper the base flow of such an inclined buoyancy layer is solved analytically for arbitrary Prandtl numbers. By applying linear stability analyses, five unstable modes are identified for both the fixed temperature and the isoflux boundary conditions, i.e., the stationary longitudinal roll (LR) mode, the oblique roll with low streamwise wave-number (OR-1) and high streamwise wave-number (OR-2) modes, and the Tolmien-Schlichting (TS) wave with low streamwise wave-number (TS-1) and high streamwise wave-number (TS-2) modes. It is indicated that the Coriolis effect induced by the rotation leads the critical modes to be three dimensional, and a larger tilt angle of the plate and stronger Coriolis effect cause both TS wave modes to be more unstable for both thermal boundary conditions. When the Coriolis effect is considered, the OR-1 and OR-2 modes are the most unstable mode at low and high tilt angles, respectively, but the TS-1 wave mode may be the most unstable one when the plate is nearly vertical. In addition, the spanwise phase velocities of the TS wave modes change directions as the tilt angle passes some threshold values for both thermal boundary conditions except for the TS-1 wave mode with a fixed temperature boundary condition, which propagates in the same spanwise direction for all explored tilt angles.

DOI: 10.1103/PhysRevE.108.025102

## I. INTRODUCTION

A buoyancy-driven boundary layer or buoyancy layer near a cooled or heated inclined plate immersed in a stably stratified fluid is a classical model in meteorology and oceanography. For example, katabatic winds are formed when the mountain surface becomes colder than the surrounding air, and plumes occur beneath floating ice shelves and at the front of tide water glaciers [1]. Prandtl [2] first introduced this model to analyze valley and mountain winds, where a parallel flow solution is derived with a reversal in the velocity profile. For its applications in meteorology we refer to the book by Stull [3]. It was shown experimentally and numerically that such kinds of buoyancy layers can be formed near the vertical sides of a cavity, which are maintained at different temperatures [4,5]. Gill and Davey [6] investigated the linear stability of such a buoyancy layer near a vertical wall, and the inclined case was first analyzed by Iyer [7], who found two types of instabilities: the transverse (streamwise periodic) traveling Tolmien-Schlichting (TS) waves and the longitudinal (spanwise periodic) rolls (LR). Later on, the spatiotemporal stability and the transition to unsteadiness of natural convection near vertical walls are studied numerically and theoretically [8–10], and most previous studies focused on the transverse TS wave mode [11]. Based on three-dimensional stability analyses of Prandtl's buoyancy layer, an oblique-roll (OR) mode is found to be more unstable than the transverse TS wave mode and the LR mode at some inclination angles and Prandtl numbers because of the ambient thermal stratification [12], and may be subject to transient growth [13].

In high latitudes and on long glaciers, a cross-slope wind occurs and the rotation-induced Coriolis effect on the katabatic flow must be considered. In order to understand the circulation induced by cooling of the air at the slopes of Antarctica, a one-dimensional model of the boundary-layer flow was developed for the unit Prandtl number, and the base flow solution was solved for a stably stratified ambient medium [14]. Recently, some models were proposed to include the Coriolis effect in the buoyancy layer, and showed at the far field that the temperature did not approach asymptotically to the background value [15] and the wall-normal velocity did not vanish [16], suggesting an unstable background stratification. However, aircraft-based field measurement of katabatic wind over the Greenland ice sheet illustrates stably stratified buoyancy layers and circumstance [17]. Therefore, there are different opinions on whether there exists a tilt buoyancy layer in a stably stratified rotating medium, and this is the main motivation of the present paper.

## II. PHYSICAL MODEL AND METHODS

We consider the Prandtl buoyancy layer near a flat plate inclined at an angle $\chi$ with respect to the horizontal. The system is rotating about a vertical axis with angular velocity

*jjtao@pku.edu.cn

 

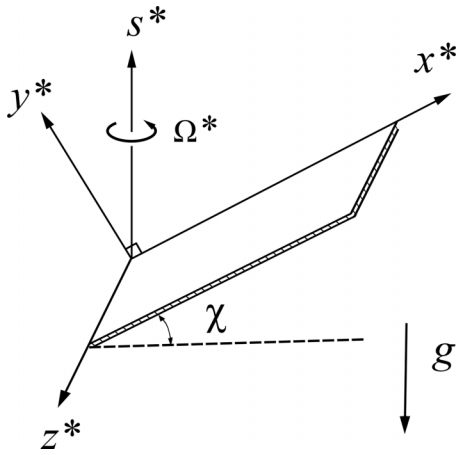


FIG. 1. Schematic geometry of an inclined buoyancy layer rotating about an axis parallel to the direction of gravity.

$\Omega^*$ as shown in Fig. 1. The temperature in the ambient fluid $T^*_\infty(s^*)$ varies linearly in the vertical direction,

$$T^*_\infty(s^*) = T^*_\infty(0) + N^*_\infty s^*, \tag{1}$$

where $s^*$ is measured vertically opposite to the direction of gravity $\mathbf{g}$. $N^*_\infty$ is the temperature gradient in the medium. We consider the katabatic winds, which means the mountain or glacier surface is colder than the surrounding air, forcing the wind to rush down the slope. The wall temperature is decreased by a fixed amount $\Delta T^*$ below that of the fluid outside the boundary layer. The coordinates $x^*$ and $y^*$ are parallel and normal to the wall, while $z^*$ points in the spanwise direction. The subscript "$\infty$" and the superscript "$*$" denote the ambient condition and dimensional quantities, respectively.

The governing equations in the Boussinesq approximation are given by

$$\begin{aligned}\frac{\partial \mathbf{V}^*}{\partial t^*} + \mathbf{V}^*\cdot\nabla\mathbf{V}^* + 2\boldsymbol{\Omega}^*\times\mathbf{V}^* &= -\nabla(P^*/\rho_r) - \mathbf{g}\gamma(T^*-T^*_\infty) \\ &\quad + \nu\nabla^2\mathbf{V}^*, \\ \frac{\partial T^*}{\partial t^*} + \mathbf{V}^*\cdot\nabla T^* &= \kappa\nabla^2 T^*, \\ \nabla\cdot\mathbf{V}^* &= 0,\end{aligned} \tag{2}$$

where $\rho_r$, $\nu$, $\kappa$, and $\gamma$ are the reference fluid density corresponding to $T^*_\infty(0)$, the kinematic viscosity, the thermal diffusivity, and the coefficient of thermal expansion, respectively.

In the following, the dimensionless variables are defined as

$$\begin{aligned}(X, Y, Z) &= \frac{(x^*, y^*, z^*)}{d}, \quad t = \frac{t^*\nu}{d^2}, \\ T &= \frac{T^* - T^*_\infty}{\Delta T^*}, \quad d = \left[\frac{4\nu\kappa}{g\gamma\sin^2(\chi)N^*_\infty}\right]^{1/4}.\end{aligned} \tag{3}$$

The dimensionless parameters of this flow system are the Grashof number $G$, the Coriolis number $\tau$, and the Prandtl number Pr,

$$G = \frac{g\gamma\sin(\chi)\Delta T^* d^3}{\nu^2}, \quad \tau = \Omega^* d^2/\nu, \quad \mathrm{Pr} = \frac{\nu}{\kappa}.$$

The nondimensional variables are $U = U_0 + u$, $V = V_0 + v$, $W = W_0 + w$, and $T = \theta_0 + \theta$, where $u$, $v$, $w$, $\theta$ are perturbations and $U_0$, $V_0$, $W_0$, and $\theta_0$ constitute the undisturbed base flow solution. Prandtl [2] found that in the case $\tau = 0$, the base flow is directed in the $X$ direction and the velocity and the temperature profile are functions of the distance from the boundary, i.e.,

$$\begin{aligned}U_0 &= -\frac{G}{2}e^{-Y}\sin(Y), \quad V_0 = W_0 = 0, \\ \theta_0 &= -e^{-Y}\cos(Y).\end{aligned} \tag{4}$$

Inspired by the Prandtl's solution, we consider the rotation effect and assume that the boundary layer is a parallel flow, i.e., $V_0 = 0$ and $U_0$, $W_0$, and $\theta_0$ are functions of $Y$. After applying the following boundary conditions,

$$U_0(0) = W_0(0) = \theta(0) + 1 = U_0(\infty) = \theta_0(\infty) = 0, \tag{5}$$

the base flow solution of the rotating buoyancy layer can be solved as

$$\begin{aligned}U_0 &= -\frac{G}{2}\mu^2 e^{-\mu Y}\sin(\mu Y), \\ V_0 &= 0, \\ W_0 &= \frac{G}{2}\tau\cos(\chi)[e^{-\mu Y}\cos(\mu Y) - 1], \\ \theta_0 &= -e^{-\mu Y}\cos(\mu Y),\end{aligned} \tag{6}$$

where $\mu$ is defined by

$$\mu \equiv \{1 + [\tau\cos(\chi)]^2\}^{1/4}. \tag{7}$$

Note that using $G$ instead of the Rayleigh number $\mathrm{Ra} = G\,\mathrm{Pr}$ as the control parameter, the dimensionless base flow solution is independent of Pr. Different from the previous solutions [15,16], the present temperature difference from the surroundings $\theta_0$ vanishes in the far field and the wall-normal velocity is zero, corresponding to a stably stratified ambient fluid, a result consistent with the field measurement of katabatic wind over the Greenland ice sheet [17]. It is checked that the solution of the previous one-dimensional mode [14] is a special case of the present solution at $\mathrm{Pr} = 1$, and when the Coriolis effect is excluded or $\tau = 0$, the base flow solution [Eqs. (6)] is reduced to the Prandtl solution [2].

In the following stability analysis, the normal mode of infinitesimal disturbance is represented as

$$\begin{Bmatrix} u \\ v \\ w \\ \theta \end{Bmatrix} = \begin{Bmatrix} \frac{i\alpha}{k^2}\Phi'(Y) + \Psi(Y) \\ \Phi(Y) \\ \frac{i\beta}{k^2}\Phi'(Y) - \frac{\alpha}{\beta}\Psi(Y) \\ \Theta(Y) \end{Bmatrix} e^{i(\alpha X + \beta Z - \omega t)}, \tag{8}$$

where $k^2 = \alpha^2 + \beta^2$, and $\alpha$ and $\beta$ are the streamwise and spanwise wave numbers, respectively. $\Phi(Y)$, $\Psi(Y)$, and $\Theta(Y)$ are the eigenfunctions of normal velocity, normal vorticity,

and disturbance temperature, respectively, and the prime $'$ represents $d/dY$. Introducing the above mode into the linearized governing equations, we have

$$\left(\frac{\beta^2}{k^2}U_0' + \frac{-\alpha\beta}{k^2}W_0'\right)\Phi + i(\alpha U_0 + \beta W_0 - \omega)\Psi + \frac{2\tau\beta}{k^2}(i\cos\chi\,\Phi' - \alpha\sin\chi\,\Phi) = \Psi'' - k^2\Psi + G\frac{\beta^2}{k^2}\Theta,$$

$$(\Phi'' - k^2\Phi)(i\alpha U_0 + i\beta W_0 - i\omega) - i(\alpha U_0'' + \beta W_0'')\Phi = \frac{2\tau k^2}{\beta}(-i\cos\chi\,\Psi' + \alpha\sin\chi\,\Psi) + \Phi'''' - 2k^2\Phi'' + k^4\Phi - i\alpha G\Theta' - k^2 G\,\mathrm{ctg}\,\chi\,\Theta,$$

$$\Theta'' - k^2\Theta - i(\alpha U_0 + \beta W_0 - \omega)\mathrm{Pr}\,\Theta = \frac{4}{G}\left(\frac{i\alpha}{k^2}\Phi' + \Psi + \mathrm{ctg}\,\chi\,\Phi\right) + \mathrm{Pr}\,\theta_0'\Phi, \qquad (9)$$

with the following boundary conditions,

$$\Psi(0) = \Phi'(0) = \Phi(0) = \Theta(0) = 0,$$
$$\Psi(\infty) = \Phi'(\infty) = \Phi(\infty) = \Theta(\infty) = 0, \qquad (10)$$

where the prime $'$ indicates $d/dY$.

Equations (9) and (10) constitute an eighth-order differential equation with eight boundary conditions, an eigenvalue problem governing the dispersion relationship

$$\mathcal{F}(\omega, \alpha, \beta; G, \tau, \chi) = 0, \qquad (11)$$

which are solved by a spectral collocation method based on Chebyshev polynomials. A value of $Y_{\max}$ of 30 was found to be sufficiently large for all unstable modes discussed in this paper. The eigenfunctions expanded in Chebyshev series are substituted into Eqs. (9) and (10), which are applied at the Gauss-Lobatto points and are solved by the QZ method [18]. The number of Chebyshev polynomials is 100, which was found to be large enough to obtain consistent eigenvalues of the buoyancy layer with the Coriolis effect. In addition, the effect of a uniform-heat-flux or isoflux boundary condition on the unstable modes is discussed as well, and $\Theta'(0) = 0$ will be used in conditions Eqs. (10) instead of $\Theta(0) = 0$.

In this paper, temporal stability analyses are carried out, and the neutral states, where the wave numbers and the frequency are set to be real, are mainly discussed because they separate the stable and unstable states. The onset of instability occurs first at the critical state, where the Grashof number reaches its local minimum value $G_c$, and the corresponding critical wave numbers and frequency $(\alpha_c, \beta_c, \omega_c)$ can be obtained simultaneously for three kinds of unstable modes, i.e., the traveling TS waves with zero $\beta$, the longitudinal rolls with zero $\alpha$, and the oblique-roll mode.

## III. RESULTS AND DISCUSSION

Without the Coriolis effect or in the limit $\tau = 0$, $W_0 = 0$, and Eqs. (9) degenerates to Eqs. (4) in Tao [12], which owns the same eigenfunctions for $(\alpha, \beta, \omega)$ and $(\alpha, -\beta, \omega)$ at any given $G$. It is noted that the present work discusses the katabatic winds, the downslope flows due to the cooled plates, while Tao's basic solution is for anabatic winds, where the flow direction is upward along the inclined heated plate. According to the definition, the Coriolis number $\tau$ is close to infinity as the tilt angle $\chi$ approaches zero, and when $\chi$ is larger than $2^\circ$, $\tau$ at any latitude is less than 0.5 for the atmosphere. Therefore, only $\mathrm{Pr} = 0.72$ and the effect of $\tau \leqslant 0.5$ are considered in this paper.

### A. Coriolis effect for plate with fixed temperature

In comparison with the Prandtl buoyancy layer, the additional Coriolis term in Eq. (2) brings multiple influences, e.g., acting as a driving force to cause the cross flow and then change the base flow, and providing an additional force normal to the tilted plate and then affecting the flow instabilities. For buoyancy layers with a fixed temperature boundary condition, i.e., $\Theta(0) = 0$, the isocontours of $G$ in the $\alpha$-$\beta$ space are shown in Fig. 2 for the neutral states at $\chi = 40^\circ$ and different Coriolis numbers $\tau$.

According to the linear stability analysis, whenever there is a critical Grashof number, above which there will be its corresponding unstable mode. When $\tau = 0$, it is shown in Fig. 2(a) that there are three unstable modes, i.e., the longitudinal roll (LR) mode, the TS wave mode with a lower streamwise wave number (TS-1), and the TS wave mode with a higher streamwise wave number (TS-2), whose critical parameters $(G, \alpha, \beta, \omega)$ are $(62.38, 0, 0.488, 0)$, $(324.53, 0.192, 0, -9.96)$, and $(331.93, 0.501, 0, -14.93)$, respectively, and show several features. First, at the critical state of the LR mode, where the Grashof number reaches its local minimum, the critical frequency is zero, representing a stationary mode. Second, for katabatic flows without a rotation effect, the two TS wave modes are two dimensional ($\beta = 0$) as marked in Fig. 2(a). Similar phenomena have been found for other buoyancy-driven boundary-layer flows [6,19], where it is explained that the TS-1 mode is controlled by the buoyancy-driven mechanism and the TS-2 mode is governed by the shear-driven mechanism.

The dimensional thickness of the buoyancy layer is approximately $5d$, which can be obtained from Eqs. (6). Note that the critical Grashof number is the ratio of buoyancy force to viscous force, and $\tau$ is the reciprocal of the Eckman number and represents the ratio of Coriolis force to viscous force. As discussed above, the critical Grashof numbers for the buoyancy layers are much higher than 1 while $\tau$ is considered to be less than 1, and hence in the present configuration the buoyancy force is much higher than the Coriolis force, and the present buoyancy layer is intrinsically different from the Eckman layer, where the Coriolis force is necessary and is balanced by the viscous force. According to the normalized eigenfunctions of the three modes shown in Fig. 3,

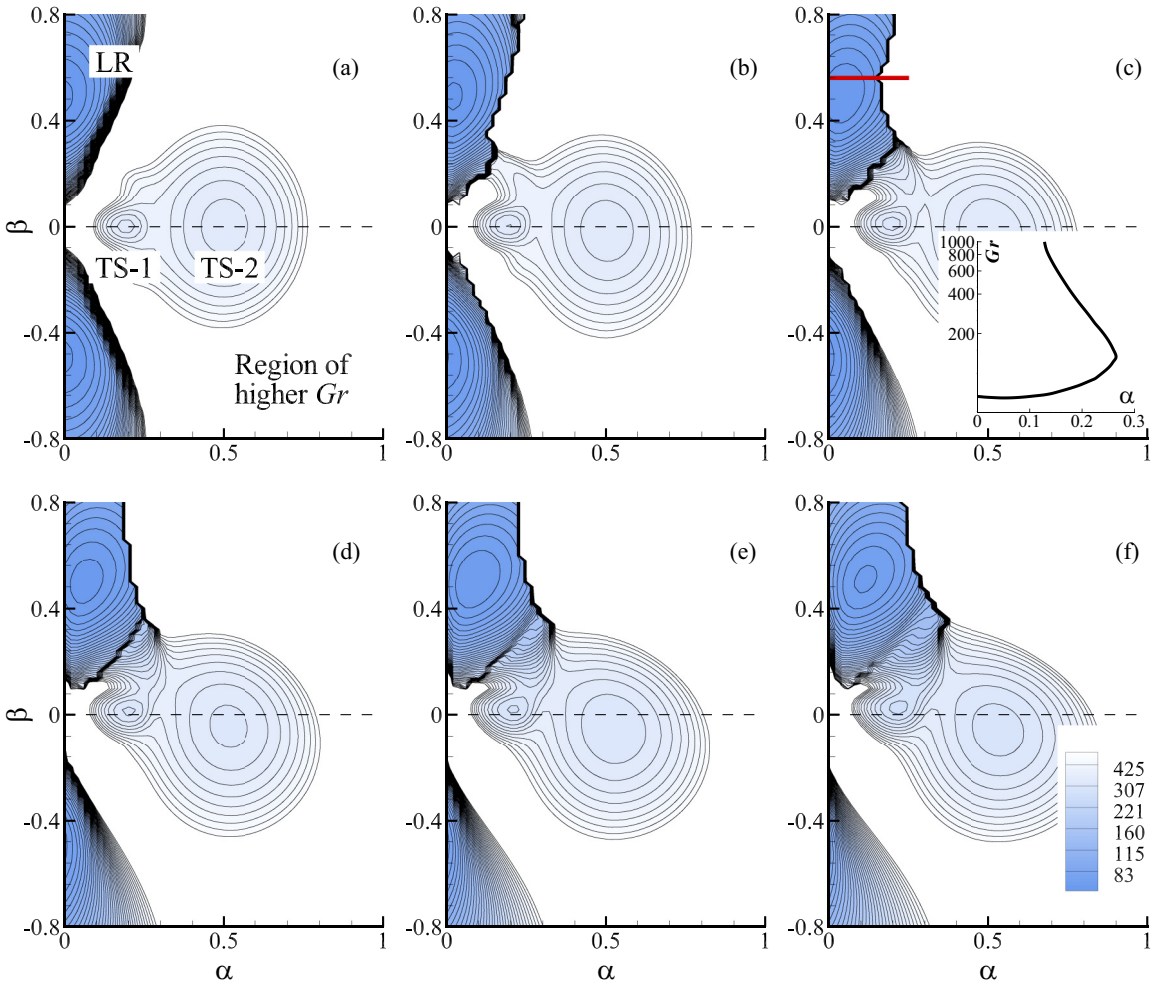


FIG. 2. Isocontours of the Grashof number at neutral state for $\chi = 40^\circ$ and the Coriolis number (a) $\tau = 0$, (b) $\tau = 0.1$, (c) $\tau = 0.2$, (d) $\tau = 0.3$, (e) $\tau = 0.4$, and (f) $\tau = 0.5$, respectively. The critical parameters for the LR, TS-1, and TS-2 modes labeled in (a) are $(G, \alpha, \beta, \omega) = (62.38, 0, 0.488, 0)$, $(324.53, 0.192, 0, -9.96)$, and $(331.93, 0.501, 0, -14.93)$, respectively. Since modes with larger $G$ are more stable and of less interest, the contours for $G > 500$ are not shown. The inset of (c) represents the neutral curve for $\beta = 0.56$ marked with the thick red solid line.

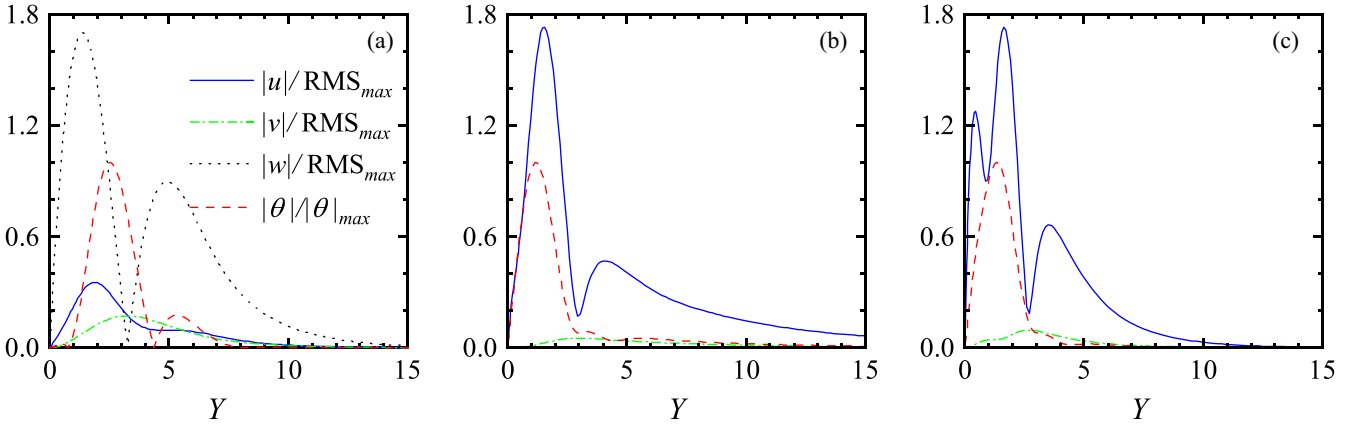


FIG. 3. Normalized critical eigenfunction profiles at $\chi = 40^\circ$ and $\tau = 0$ for (a) LR mode, (b) TS-1 mode, and (c) TS-2 mode with the fixed temperature boundary condition. RMS represents the root-mean-square of the disturbance velocity, and the subscript max indicated the maximum.

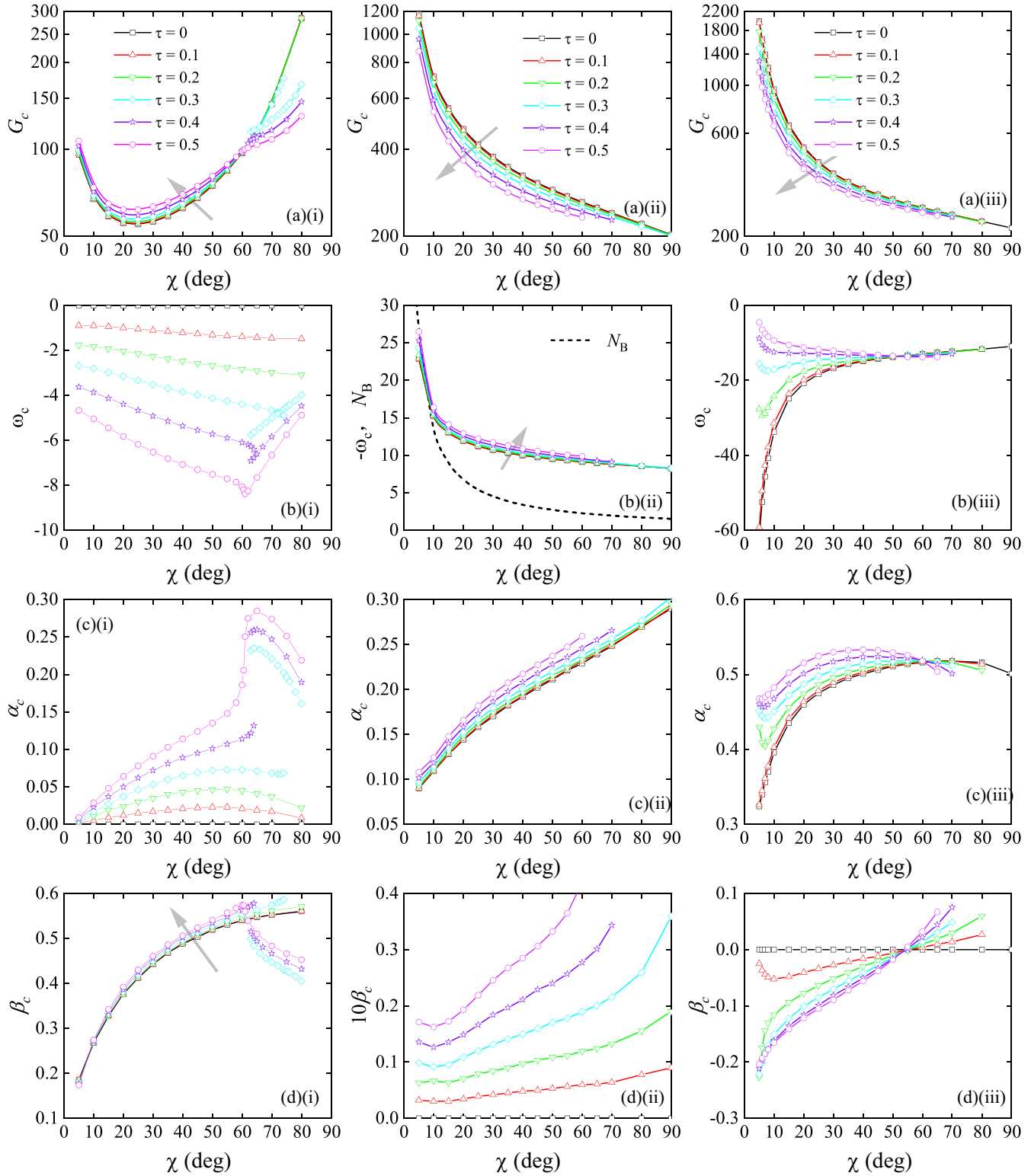


FIG. 4. The critical parameters obtained at different Coriolis numbers $\tau$ and tilt angles $\chi$ are shown in the left, middle, and right columns for the oblique-roll modes, TS-1 mode, and TS-2 mode with the fixed temperature boundary condition, respectively. The gray arrows indicate the variation directions of the parameters with the increase of $\tau$.

the TS-2 mode is confined in the buoyancy layer, while the perturbations of the LR and TS-1 modes penetrate into the stably stratified medium three times farther than the thickness of the buoyancy layer.

With the increase of $\tau$, the isocontours of $G$ for the neutral states evolve differently for different modes as shown in Figs. 2(b)–2(f). For the LR mode at $\chi = 40^\circ$, increasing $\tau$ leads to a right movement of the local minimum of $G$ in the

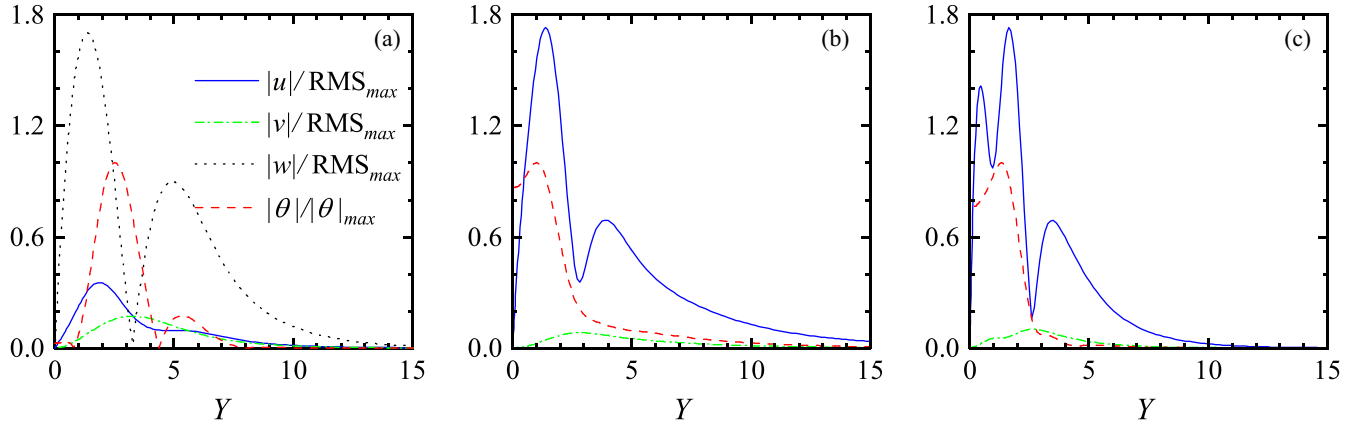


FIG. 5. Normalized critical eigenfunction profiles at $\chi = 40^\circ$ and $\tau = 0$ for (a) LR mode, (b) TS-1 mode, and (c) TS-2 mode with the isoflux boundary condition. RMS represents the root-mean-square of the disturbance velocity, and the subscript max indicated the maximum.

$\alpha$-$\beta$ space, and hence the stationary longitudinal roll mode changes to a three-dimensional traveling oblique-roll (OR-1) mode due to the Coriolis effect. The evolution of two TS wave modes has contrary trends, i.e., $\beta_c$ of the TS-1 and TS-2 modes increases and decreases with the increase of $\tau$ at $\chi = 40^\circ$, respectively, indicating that these two-dimensional TS wave modes change to three-dimensional ones. It is noted that $G$ at the neutral state is not a single-valued function of the wave-number vector. The thick solid line segment shown in Fig. 2(c) corresponds to the neutral curve illustrated in the inset, where the same wave-number vector, e.g., $(\alpha, \beta) = (0.2, 0.56)$, has different neutral-state Grashof numbers.

The effects of the Coriolis number and the tilt angle on the critical parameters of different modes are summarized in Fig. 4, and several characteristics should be noted. First, a larger tilt angle $\chi$ and stronger Coriolis effect lead the buoyancy layer to be more unstable to both TS wave modes, while $G_c$ of the OR-1 mode decreases first then increases with the augment of $\chi$. According to the present analyses, the OR-1 mode is the most unstable mode at low and moderate tilt angles, e.g., $\chi < 60^\circ$. Second, the effects of $\tau$ and $\chi$ on the critical wave numbers are quite different for the TS-1 and TS-2 modes. For the TS-1 mode, stronger rotation or higher $\tau$ leads to larger $\alpha_c$ and $\beta_c$, and larger $\chi$ corresponds to larger $\alpha_c$ and $\beta_c$ as well when $\chi > 10^\circ$. However, for the TS-2 mode, increasing $\tau$ enhances and decreases $\alpha_c$ when $\chi$ is less and larger than $60^\circ$, respectively, but decreases and increases $\beta_c$ as $10^\circ < \chi < 55^\circ$ and $\chi > 55^\circ$, respectively. Consequently, when the tilt angle of the plate passes $55^\circ$, the TS-2 mode changes its spanwise traveling direction due to the Coriolis effect. Third, the critical frequency $\omega_c$ of the TS-2 mode is affected by $\tau$ only at small tilt angles, e.g., $\chi < 45^\circ$, and $\omega_c$ of TS-1 is nearly independent of $\tau$ at different tilt angles. As shown in Fig. 4(b)(ii), $-\omega_c$ decreases monotonically in a similar way as $N_B = \frac{2}{\sin\chi} P^{-1/2}$, the Brunt-Väisälä or buoyancy frequency of the internal wave in the ambient fluid, and even coincides with $N_B$ at small tilt angles, reflecting the buoyancy-driven mechanism. In the previous study on the anabatic flow [12], the buoyancy frequency coincides with the critical frequency of not the TS wave mode but the OR mode when $\chi > 22^\circ$. It is mentioned that the frequency of the TS wave mode shown in Fig. 5(c) of Ref. [12] is $\omega_c G_c^{1/5} P^{-1/4}$, not the critical frequency $\omega_c$. Fourth, at large tilt angles, e.g., $\chi > 60^\circ$, a new oblique-roll mode emerges due to the Coriolis effect, which has a lower $G_c$ than that of the OR-1 mode and becomes the most unstable mode when $\tau$ and $\chi$ are large enough, and is referred to as the OR-2 mode hereafter. The OR-2 mode has a larger $\alpha_c$ but a smaller $\beta_c$ than those of the OR-1 mode for the same base flow. Increasing $\tau$ will increase the $\omega_c$, $\alpha_c$, and $\beta_c$ of both oblique-roll modes, but different from the OR-1 mode, enlarging $\chi$ will increase the $\omega_c$ and decrease the $\beta_c$ of the OR-2 mode.

### B. Coriolis effect for isoflux plate

The Prandtl-type buoyancy layers have a special feature, i.e., the velocities and temperature of the basic state only vary in the normal direction [Eqs. (4) and (6)] and hence it has a uniform heat flux or isoflux boundary due to the fact that $\theta_0'(0) = \mu$. Therefore, when the unstable boundary layer retains the isoflux boundary condition, we have $\Theta'(0) = 0$ instead of $\Theta(0) = 0$, and the corresponding linear instabilities are analyzed and discussed as follows.

For a mode with $\alpha = 0$, $\Theta'$ does not appear explicitly in Eq. (9), then the eigenvalues for different temperature boundary conditions would be very close to each other when the temperature perturbations are small near the wall. For example, the critical parameters for the LR mode with the isoflux boundary condition at $\chi = 40^\circ$ and $\tau = 0$ are $(G, \alpha, \beta, \omega) = (62.38, 0, 0.489, 0)$, which almost coincide with those solved for the fixed temperature condition. As shown in Fig. 5, the corresponding eigenfunctions are nearly the same as those shown in Fig. 3 except for the $\theta$ curve near the wall ($Y = 0$). For modes with $\alpha \neq 0$, the term $i\alpha G\Theta'$ in Eq. (9) makes the linearized momentum equations at $Y = 0$ different for different temperature boundary conditions, leading to quantitatively different eigenvalues and eigenfunctions. For example, $(G, \alpha, \beta, \omega)$ of the TS-1 and TS-2 modes with the isoflux boundary condition are $(138.55, 0.279, 0, -6.72)$ and $(364.55, 0.546, 0, -17.26)$ at $\chi = 40^\circ$ and $\tau = 0$, respectively.

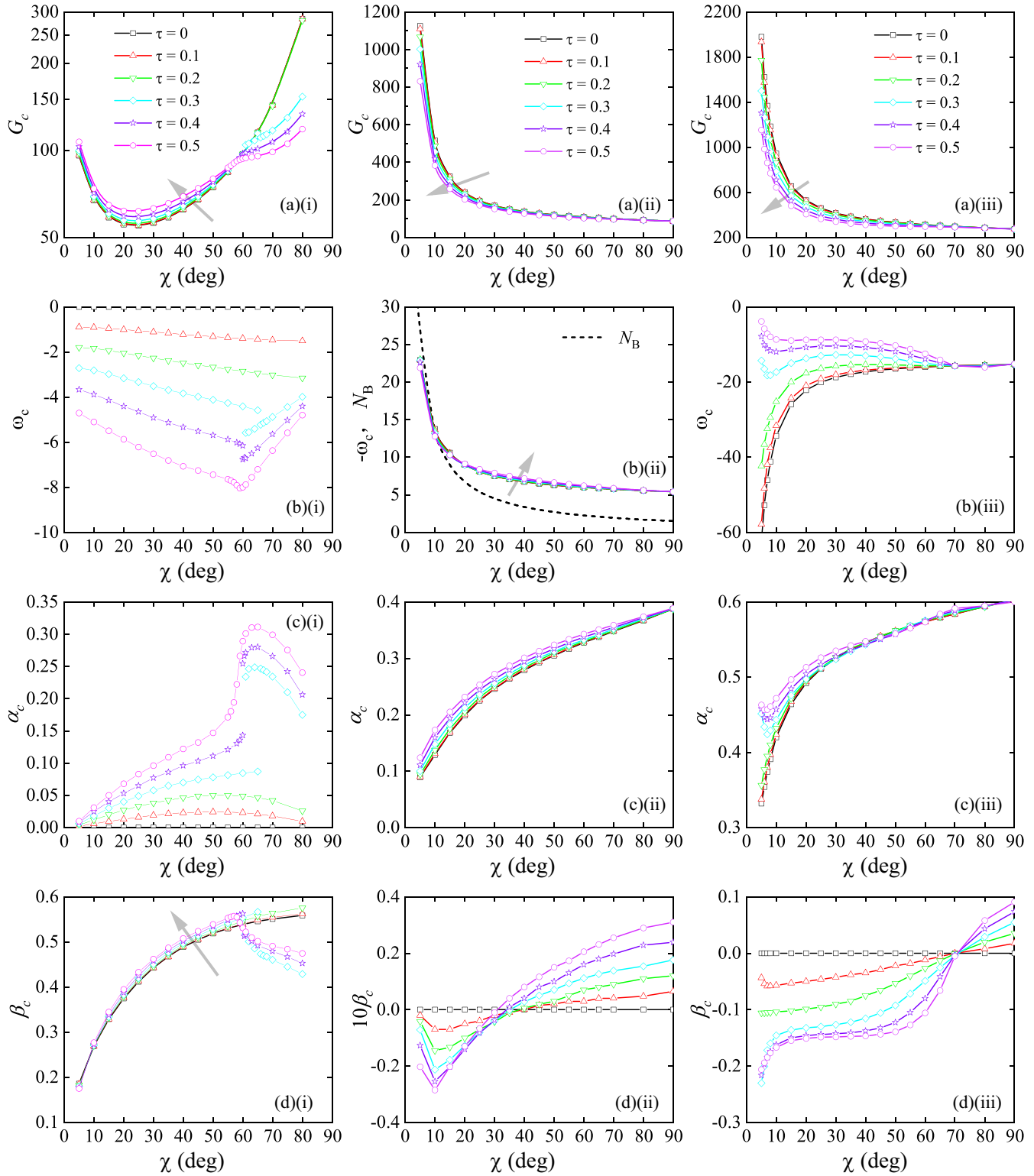


FIG. 6. The critical parameters obtained at different Coriolis numbers $\tau$ and tilt angles $\chi$ are shown in the left, middle, and right columns for the oblique-roll modes, TS-1 mode, and TS-2 mode with the isoflux boundary condition, respectively. The gray arrows indicate the variation directions of the parameters with the increase of $\tau$.

Since the base flow solution is the same for cases with these two kinds of temperature boundary conditions, the unstable modes and the relations between the critical parameters and the configurations (e.g., $\chi$ and $\tau$) are similar as shown in Fig. 6, e.g., there are five unstable modes, the LR, OR-1, OR-2, TS-1, and TS-2 modes. The main qualitative difference lies in the critical spanwise wave number of the TS-1 mode as shown in Fig. 6(d)(ii), where a stronger Coriolis effect

or higher $\tau$ leads to lower $\beta_c$ as $\chi < 30^\circ$ for the isoflux boundary condition, while for a fixed temperature condition [$\Theta(0) = 0$] increasing $\tau$ will enlarge $\beta_c$ at all explored tilt angles [Fig. 4(d)(ii)]. Therefore, with the isoflux boundary condition, the spanwise phase velocities of the TS-1 mode are different for the plates with small and large tilt angles. In addition, when the boundary plate is nearly vertical, it is shown in Fig. 6 that the most unstable mode is the TS-1 mode in the explored parameter space, not the oblique-roll modes.

## IV. CONCLUSION

A katabatic boundary-layer flow will be formed if a cooled slope is immersed in a thermally stratified ambient medium. When such a buoyancy layer is subjected to a rotation with the axis parallel to the direction of gravity, e.g., the glacier wind at high latitudes, the Coriolis force has important influences on the base flow and its hydrodynamic instabilities. To the best of our knowledge, the stability of such a katabatic buoyancy layer has yet to be studied theoretically. Different from the previous models, the present model is for arbitrary Prandtl numbers and the ambient thermal stratification is not disturbed by the base flow of the buoyancy layer. There are a total of five unstable modes revealed by the linear stability analyses for both the fixed temperature and the isoflux thermal boundary conditions. When the Coriolis effect caused by rotation is included, the stationary longitudinal roll (LR) mode will change to the oblique-roll mode (OR-1), and both TS wave modes change from two dimensional to three dimensional. For both TS wave modes at both thermal boundary conditions, increasing the Coriolis parameter $\tau$ decreases their critical Grashof numbers $G_c$ at different tilt angles $\chi$ of the boundary, indicating that the rotation destabilizes the TS wave modes. The Coriolis effect on the oblique-roll modes, however, shows different features: Enhancing the rotation or increasing $\tau$ stabilizes the OR-1 mode at low and moderate tilt angles, but destabilizes the OR-2 mode at large tilt angles, and hence OR-2 becomes more unstable than OR-1 at large $\chi$ and $\tau$. It is found that the Brunt-Väisälä frequency coincides with the critical frequency of the TS-1 mode when $\chi \lessapprox 10^\circ$, suggesting a strong connection between the oscillatory behavior of the TS-1 mode and the internal waves for small tilt angles. In addition, the rotation has strong effects on the critical wave numbers or phase velocities as well. For example, increasing $\tau$ will decrease the critical spanwise wave numbers of the TS wave modes with the isoflux boundary condition and the TS-2 wave mode with the fixed temperature boundary condition at low tilt angles, but increase them at large tilt angles. These encouraging results are expected to be helpful in understanding the meteorological phenomena at high latitudes.

## ACKNOWLEDGMENT

The work has been supported by the National Natural Science Foundation of China (Grants No. 91752203 and No. 11490553).

[1] I. J. Hewitt, Annu. Rev. Fluid Mech. **52**, 145 (2020).
[2] L. Prandtl, *Essentials of Fluid Dynamics* (Blackie, London, 1952).
[3] R. B. Stull, *An Introduction to Boundary Layer Meteorology* (Academic Press, New York, 1989).
[4] J. W. Elder, J. Fluid Mech. **23**, 77 (1965).
[5] A. E. Gill, J. Fluid Mech. **26**, 515 (1966).
[6] A. E. Gill and A. Davey, J. Fluid Mech. **35**, 775 (1969).
[7] P. A. Iyer, Boundary-Layer Meteorol. **5**, 53 (1973).
[8] J. Tao, P. LeQuéré, and S. Xin, J. Fluid Mech. **518**, 363 (2004).
[9] J. Tao, P. LeQuéré, and S. Xin, Phys. Rev. E **70**, 066311 (2004).
[10] P. LeQuéré, Int. J. Therm. Sci. **176**, 107430 (2022).
[11] B. Gebhart, Y. Jaluria, R. L. Mahajan, and B. Samumakia, *Buoyancy Induced Flows and Transport* (Hemisphere, London, 1988).
[12] J. Tao and F. H. Busse, Eur. J. Mech. B/Fluids **28**, 532 (2009).
[13] X. Xiong and J. Tao, Appl. Math. Mech.-Engl. Ed. **38**, 779 (2017).
[14] J. Egger, J. Atmos. Sci. **42**, 1859 (1985).
[15] I. Stiperski, I. Kavčič, B. Grisogono, and D. Durran, Q. J. R. Meteorol. Soc. **133**, 101 (2007).
[16] A. Shapiro and E. Fedorovich, Q. J. R. Meteorol. Soc. **134**, 353 (2008).
[17] G. Heinemann, Boundary-Layer Meteorol. **93**, 75 (1999).
[18] P. J. Schmid and D. S. Henningson, *Stability and Transition in Shear Flows* (Springer, Berlin, 2001).
[19] J. J. Tao and D. C. Yan, Commun. Nonlinear Sci. Numer. Simul. **4**, 34 (1999).